Inorganic Chemistry

Article

pubs.acs.org/IC

Facile Synthesis of Water-Soluble Zn-Doped $AgIn_5S_8$/ZnS Core/Shell Fluorescent Nanocrystals and Their Biological Application

Jiangluqi Song,[†] Tongtong Jiang,[†] Tianyi Guo,[†] Ling Liu,[‡] Huijie Wang,[†] Tongyan Xia,[†] Wenting Zhang,[†] Xuecheng Ye,[†] Mingya Yang,[§] Lixin Zhu,*[,§] Ruixiang Xia,*[,∥] and Xiaoliang Xu*[,†]

[†]Key Laboratory of Strongly-Coupled Quantum Matter Physics, Chinese Academy of Sciences, and Department of Physics, University of Science and Technology of China, Heifei, Anhui 230026, China

[‡]School of Science, Tianjin Polytechnic University, Tianjin 300387, China

[§]Center Laboratory and [∥]Department of Hematology, First Affiliated Hospital of Anhui Medical University, Heifei 230026, China

Supporting Information

ABSTRACT: Here we demonstrate a novel and facile strategy of highly luminescent water-soluble Zn-doped $AgIn_5S_8$ (ZAIS) nanocrystals and ZAIS/ZnS core/shell structures, which were based on hydrothermal reaction between the acetate salts of the corresponding metals and sulfide precursor in the presence of L-cysteine at 110 °C in a Teflon-lined autoclave. The photoluminescent (PL) emission wavelength can be conveniently tuned from 560 to 650 nm by tailoring the stoichiometric ratio of [Ag]/[Zn]. The as prepared nanocrystals were characterized systematically and exhibit long PL lifetimes more than 100 ns. The influence of experimental conditions, including concentration of L-cysteine and reaction temperature, was investigated. In addition, we performed a coating procedure with the ZnS shell outside the ZAIS core and showed excellent PL quantum yields up to 35%. The *in vitro* experiment exhibited quite low cytotoxicity and marvelous biocompatibility, revealing their promising prospect in bioscience. Furthermore, the obtained ZAIS/ZnS nanocompounds (NCs) were covalently conjugated to alpha-fetoprotein antibodies and targeted fluorescent imaging for hepatocellular carcinoma cells was realized.

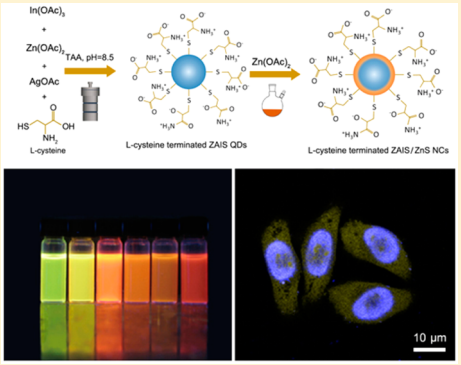

1. INTRODUCTION

Ternary I−III−VI nanocrystals, which are also called quantum dots (QDs), have gained intensive research in biolabeling, light emitting diodes, solar cells, and photocatalysis during recent decades, because of their wonderful biocompatibility, excellent optical properties, and high biochemical stability.[1−10] Among the I−III−VI QDs, Ag−In−S (AIS) nanoparticles are attracting intensive attention in the past few years for a relatively wide band gap (ranging from 1.87 to 2.03 eV) and pronounced defect tolerance.[11] Most of the reported synthetic methods were concentrated on thermolysis of various metal−sulfur precursors in the organic phase, which obtains a product with high crystallinity and PL quantum yield (QY), limiting their direct applications in bioscience.[2,12−14] Although there have been many protocols for post-treatment of phase transition via ligand exchange, these methods emerged with obvious drawbacks including being time-consuming, use of toxic chemicals, decreased QY, tedious steps, and high cost.[6,15] Hence, it is significant to develop an aqueous synthesis for Ag−In−S QDs.

Recently, Luo et al. reported a one-step synthesis of water-soluble AIS QDs with metal salts and sodium sulfide as precursors and glutathione as stabilizer. After capping with ZnS, QDs exhibited photocatalytic activities in the degradation of Rhodamine B, and the QY was improved from 3% to 15%.[4] Soon afterward, Regulacio and his co-workers prepared $AgInS_2$−ZnS QDs with poly(acrylic acid) and mercaptoacetic acid as surface ligand, which showed unsatisfactory QY of 20%.[16] Apparently, exploration of new strategies for producing highly luminescent and water-soluble ternary or quaternary QDs, which is conducive to fundamental studies and possible technical applications, is still expected.

In this paper, we report a facile aqueous method for the synthesis of Zn-doped $AgIn_5S_8$ (ZAIS) nanocrystals reacted in a Teflon-lined autoclave under 110 °C using L-cysteine as a stabilizer for the first time. The PL emission wavelength can be facilely tuned from 560 to 650 nm by changing the stoichiometric ratio of [Ag]/[Zn]. The luminescent mechanism was discussed, manifesting that the combination of intrinsic states dominated the PL emission. The key factor for the highly luminescent QDs was a suitable reaction temperature and an appropriate concentration of L-cysteine. The as prepared ZAIS QDs give QY in the range of 15−26%. With the purpose of reducing the surface defects and increasing chemical stability, we introduced a coating procedure. After coating with ZnS, the

Received: October 29, 2014
Published: January 16, 2015

DOI: 10.1021/ic502600u
Inorg. Chem. 2015, 54, 1627−1633

QY of ZAIS/ZnS nanocompounds (NCs) were further improved as high as 35%, which achieved the same level compared to water-soluble CdTe QDs, and the lifetime was longer than 200 ns. Furthermore, these ZAIS/ZnS are found to demonstrate wonderful stability and remarkable biocompatibility, conjugated with alpha-fetoprotein (AFP) antibodies and labeled to hepatocellular carcinoma cells for targeted fluorescent imaging. To our best knowledge, this is the first time for the application of hepatocellular carcinoma cell cytoplasm for fluorescence labeling using quaternary QDs, which provide a new approach for the clinical diagnosis and monitoring of liver cancer.

2. EXPERIMENTAL SECTION

2.1. Materials and Chemicals. All the chemicals were of analytical grade and used without further purification. Zinc acetate ($Zn(OAc)_2{\cdot}2H_2O$, 99.99%), silver acetate (AgOAc,99.8%), thioacetamide (TAA, 99%), sodium hydroxide (NaOH, 96%), L-cysteine (98.5%), and absolute ethanol were purchased from Sinopharm Chemical Reagent Co. Ltd. (Shanghai, China). Indium acetate ($In(OAc)_3$, 99.99%) was purchased from Alfa Aesar Chemical Reagent Co. (China). All the water used in experiments was deoxidized deionized water (18.25 MΩ·cm).

Alpha -fetoprotein (AFP) monoclonal antibody (bs-4708R), phosphate buffer saline (PBS, pH = 7.2), 1-ethyl-3-(3-(dimethylamino)propyl)carbodiimide hydrochloride (EDC, 98%), *N*-hydroxysuccinimide (NHS, 98%), 3-(4,5-dimethylthiazol-2-yl)-2,5-diphenyltetrazolium bromide (MTT), 4′,6-diamidino-2-phenylindole (DAPI), dimethyl sulfoxide (DMSO), penicillin−streptomycin, high glucose Dulbecco's modified Eagle medium (DMEM), fetal calf serum, and streptomycin were purchased from commercial sources.

2.2. Preparation of L-Cysteine Capped ZAIS QDs and ZAIS/ZnS NCs. ZAIS QDs were synthesized via hydrothermal synthetic method. Typically, 2.88 mg of AgOAc, 48.66 mg of $In(OAc)_3$, and a desired amount of $Zn(OAc)_2{\cdot}2H_2O$ were mixed with 5.5 mL of water. Then, 2 mL of 0.6 M L-cysteine was added, and NaOH solution (1 M) was introduced so that pH = 8.5 was achieved. Subsequently, 6.5 mL of 0.05 M TAA solution was rapidly injected into the mixture. The mixture was sealed in a Teflon-lined stainless steel autoclave and maintained at 110 °C under autogenous pressure for different times (30−270 min). After the liquid was naturally cooled to room temperature, ZAIS QDs were precipitated by adding excess ethanol, then ultrasonically treated for 5 min, and centrifuged for collection. The precipitates were dispersed in water or dried thoroughly for further use. (Samples of different emission wavelength were prepared by changing the molar ratio of [Ag]/[Zn] from 1:1 to 1:6.)

To prepare ZAIS/ZnS NCs, 10 mL of previously synthesized ZAIS QDs stock solution was loaded in a two-necked flask, heated to 100 °C in atmosphere, and refluxed with a condenser. Under stirring, 200 μL of 0.05 M of $Zn(OAc)_2$ solution was dropwise injected into the solution through a syringe. To monitor the reaction, aliquots of the sample were taken out at different time intervals to examine their photoluminescence spectra. The purification of ZAIS/ZnS was the same as that of ZAIS QDs. The schematic illustration of the procedure for fabrication L-cysteine stabilized ZAIS QDs and ZAIS/ZnS NCs is presented in Scheme 1.

2.3. Characterization of ZAIS QDs and ZAIS/ZnS NCs. The morphologies of nanoparticles were determined on a transmission electron microscope (TEM, model JEM-1400), and the element analyses were conducted on a high resolution TEM (HRTEM) equipped with an energy dispersive spectrometer (EDS) attachment. X-ray diffraction (XRD) measurements were conducted with Cu Kα (0.154 nm) serving as the incident radiation. The element analysis was conducted with X-ray photoelectron spectroscopy (XPS) using an ESCLAB 250 spectrometer. Fourier transform infrared (FTIR) spectra were measured on a Nicolet 6700 spectrometer with 2 cm^{-1} resolution using the KBr pellet technique. Photoluminescence (PL) spectra were obtained by using an RF-5301 fluorescence spectrophotometer. The

Scheme 1. Procedure for Fabrication L-Cysteine Stabilized ZAIS QDs and ZAIS/ZnS NCs

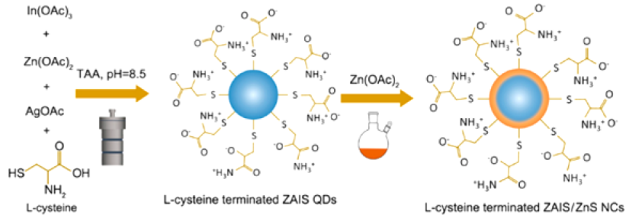

time-resolved PL spectra were performed by an Edinburgh FLS920 transient state fluorescence spectrometer. PL quantum yield (QY) was calculated using Rhodamine 6G (QY = 95%) as the standard based on the previously described method.[17]

2.4. Cell Viability. Human hepatoma cell line (Hep G2) was provided by Anhui Medical University. The cells were cultured on DMEM containing 10% of heat-inactivated fetal bovine serum (FBS) and 1% of penicillin/streptomycin at 37 °C in a humidified atmosphere with 5% CO_2. For MTT assay, the cells were seeded in 96-well plates at a density of 5×10^4 cells/mL and incubated for 24 h until cell growth reached about 80% confluence before measurement. Six of the 96 wells were set as the control group without any addition of QDs, and 6 of the 96 wells were set as the zero group only with 100 μL of DMEM. L-Cysteine stabilized ZAIS/ZnS NCs were added into each well with various concentrations ranging from 0.03 to 50 mg/mL. Cells were then incubated at 37 °C and in a 5% CO_2 atmosphere for another 24 h. Subsequently, 20 μL of MTT solutions (5 mg/mL) was added to each well, and cells were then incubated at 37 °C. After 4 h, the medium was discarded, and 150 μL of DMSO was added into each well and placed into a shaking table for 15 min to dissolve the intracellular purple formazan crystals. The absorbance of the samples was recorded at 490 nm. The cell viability was calculated by normalizing with the results obtained with no QDs loading. The complete assay above was operated thrice, and results were averaged. The same assay was performed with L-cysteine-stabilized CdTe/ZnS QDs prepared according to the previous report[18] for comparison.

2.5. Covalent Conjugation between QDs and Antibody. QDs/antibody composites were prepared via covalent linkage between QDs and antibody according to the method reported by our group[19] when their surface groups of amino and carboxyl were activated. 100 μL of QDs with yellow emission was added into 1.5 mL of PBS containing 10 μL of 10 mg/mL EDC and 15 μL of 100 mg/mL NHS, and incubated at 37 °C for 1 h in a constant temperature shaking table. After incubation, 50 μL of 1 mg/mL antibody was added to the solution, which was incubated overnight at 37 °C. The mixture was finally centrifuged and washed to remove excess QDs and reagents, and redispersed in PBS for targeted imaging.

2.6. Cell Imaging. For the fluorescent imaging, Hep G2 cells were placed in a 24-well plate at 37 °C with 5% CO_2. After 24 h incubation, 200 μL of QDs/antibodies composites was injected into each well and incubated for 4 h. After that, the DMEM medium was aspirated and the cells were washed three times with PBS. The cell nuclei were eventually stained further with DAPI for 3 min. Fluorescence images of the cells were obtained with an Olympus IX73 fluorescence microscope and Leica SP5 laser scanning confocal microscope.

3. RESULTS AND DISCUSSION

3.1. Optical Properties. It is believed that PL of I−III−VI QDs originates from the electron−hole pair emission of a defect state.[20−22] Thus, we could hardly obtain the QDs of different PL emission by changing their size like II−VI QDs.[23,24] In this study, we systematically explored the synthesis of biocompatible quaternary ZAIS QDs and ZAIS/ZnS NCs with the variation of the molar ratio of Ag/Zn from 1/6 to 1/1. Panels A−C of Figure 1 show the normalized PL spectra, digital photograph taken under UV, and the absorption spectra of

DOI: 10.1021/ic502600u
Inorg. Chem. 2015, 54, 1627−1633

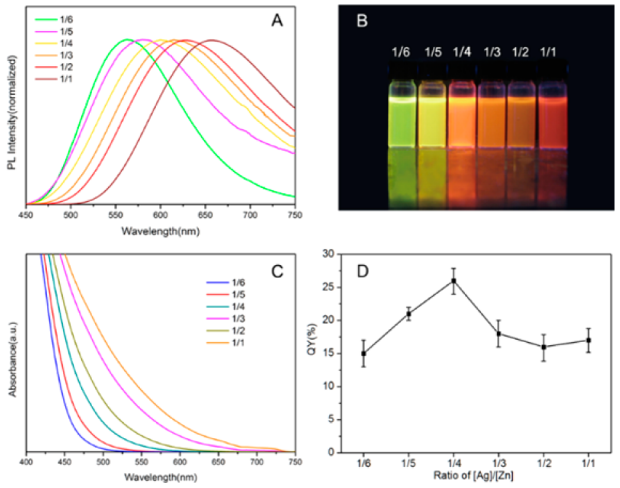

Figure 1. PL emission spectra (A), digital photograph (B), absorption spectra (C), and QY (D) of each molar ratio of [Ag]/[Zn].

ZAIS QDs with variable molar ratio of [Ag]/[Zn]. The emission peaks have a maximum intensity at a wavelength ranging from 560 to 650 nm. Different from those II−VI semiconductor nanocrystals, the PL spectrum demonstrates the typical characteristics of ternary and quaternary QDs of broad full width at half-maximum (fwhm) larger than 100 nm and asymmetry. These features may be caused by donor−acceptor transition and trap-state emission. It has been found that the conduction band of bulk Ag−In−S semiconductor is made up of hybrid orbitals of In 5p5s and S 3p, while the valence band is formed by S 3p hybridized with Ag 4d.[25] With the incorporation of Zn in the reaction system, Ag is replaced via cation exchange, leading to the decrease in the number of Ag orbitals, and expands the band gap.[26] The same reason can illustrate the absorption onset blue-shift shown in Figure 1C. All of the absorption curves exhibit broad shoulder with absorption onset located from 550 to 750 nm. No obvious exciton absorption peaks are found in the spectra coupling with the long trail on the long-wavelength region, which may be ascribed to the wide size distribution or trap-state-related emission or their combination reaction.[10] The large Stokes shift suggests that the observed PL is not a band gap emission but the emissions from surface states and intrinsic states.[13,27] As our reaction was performed in autoclaves in 110 °C, we obtained high QY ranging from 15% to 26% as is shown in Figure 1D, which may arise from the high temperature and high pressure environment contributing to QDs of high quality.

Figure 2A shows the evolution of PL emission with reaction time. The emission maximum exhibits continuous enhancement, which is ascribed to the decrease of the defect states during the progress of QD growth. Ternary I−III−VI semiconductors are known for abundant trap states which easily form interstitial atoms or vacancies and are responsible for donor−acceptor transitions.[28] Based on this cognition, deconvolution method was used to analyze the luminescence mechanism.[29,30] We deconvoluted the PL spectra (90−240 min and ZAIS/ZnS) into two Gaussian functions noted as Peak1 (shorter wavelength, around 548 nm) and Peak2 (longer wavelength, around 606 nm), which correspond to surface and intrinsic trap states, respectively, as seen in Figure 2B−H. We use integral area rather than intensity of each peak to discuss their contribution to the entire PL spectrum, because each of the two deconvoluted peaks has a distinct shape, i.e., fwhm and

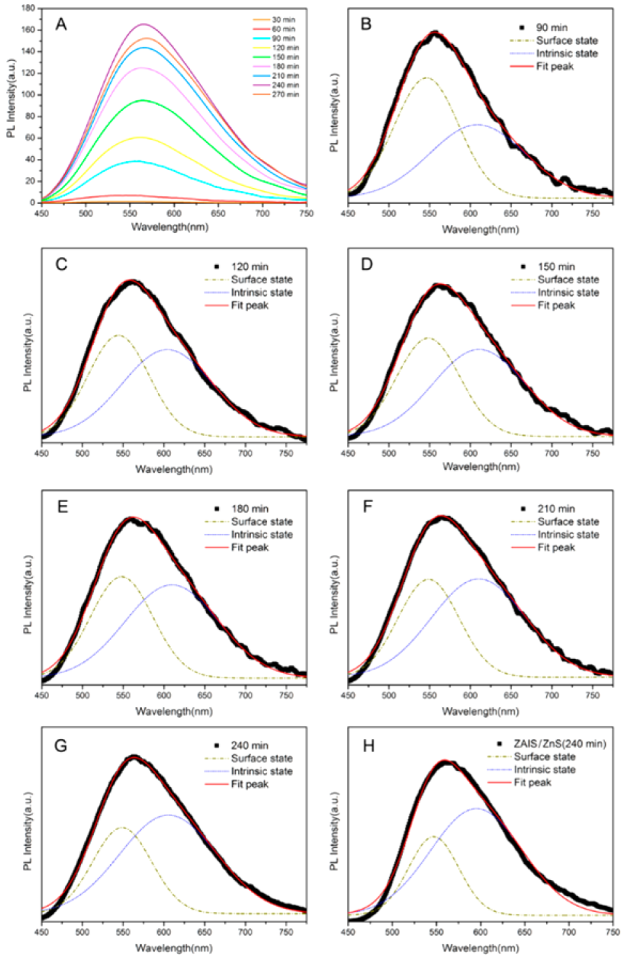

Figure 2. Evolution of PL emission of the sample [Ag]/[Zn] = 1/6 (A) and corresponding Gaussian deconvolution PL spectra with different reaction time from 90 to 240 min of ZAIS QDs (B−G) and ZAIS/ZnS NCs (240 min) (H).

peak height. We could not simply take the intensity as the indicator of their contribution. The integral area (A_1, A_2) of each function, which represents the contribution to the entire spectrum, and their specific value (A_2/A_1) are summarized in Table 1. Increasing integral area of two functions and their ratio are found, which could be explained by considering that, with the growth of the QDs, the number of shallow surface defects in high energy reduces, while the intrinsic states increase relatively.[13] After 120 min, the area of Peak2 is much larger than that of Peak1, which is similarly observed in the case of

Table 1. Summary of Integral Areas of Deconvoluted PL Peaks and Their Ratio

	integral area		
reaction time/min	Peak1	Peak2	A_2/A_1
90	3139.3	2888.5	0.92
120	4470.8	5484.9	1.23
150	7266.4	8979.8	1.24
180	9344.3	12185.5	1.30
210	10385.3	14819.5	1.43
240	10856.7	17919.6	1.65
ZAIS/ZnS[a]	30225.4	58388.2	1.93

[a]Sample is formed in situ on the as prepared ZAIS QDs (240 min).

DOI: 10.1021/ic502600u
Inorg. Chem. 2015, 54, 1627−1633

ZAIS/ZnS (Figure 2H), confirming that the surface states are further weakened and intrinsic defects working as donor−acceptor dominate the main PL emission. Thus, the high PL intensity and QY are obtained. Additional information given by Figure 2A is the decrease of PL intensity at 240 min. This could be interpreted by the further increase of surface defects, such as dangling bonds and vacancies,[31,32] providing the recombination centers and resulting in the feeblish emission.

3.2. Influence of Experimental Conditions. Zinc-doped AIS QDs were synthesized by hydrothermal protocols using L-cysteine as the stabilizer. Indium acetate and zinc acetate served as cation precursor. According to the electronic theory of acid and alkali proposed by Lewis, S^{2-} is a soft base, which can readily react with soft acid, i.e., Zn^{2+} and Ag^{+}, to form a stable product. Deng et al. found that different kinds of S sources, such as thioacetamide, sodium thiosulfate, thiourea, and sodium sulfide, have distinct reactivity.[33] Sodium thiosulfate and thiourea, which have poor reactivity, can only be hydrolyzed to release free S^{2-} by means of hydrolysis under 100 °C. However, sodium sulfide possesses a high reactivity, which can react with metal ions at room temperature, and it is hard to control reaction rate. As a consequence, TAA was used as a sulfur source.

It is reported that the optical properties of AIS and AIS/ZnS QDs depend on tailoring the experimental variables, such as pH value and the molar ratio of elements.[25,34,35] Herein, as the ZAIS QDs were synthesized using L-cysteine at 110 °C for the first time, we only focused on the dependence of PL intensity on the concentration of L-cysteine and reaction temperature in the case of ZAIS with [Ag]/[Zn] = 1/6, where we immobilized all the other experimental variables as set in the Experimental Section.

3.2.1. Effect of L-Cysteine Concentration. As is seen in Figure 3A, the PL intensity of the samples is enhanced with a

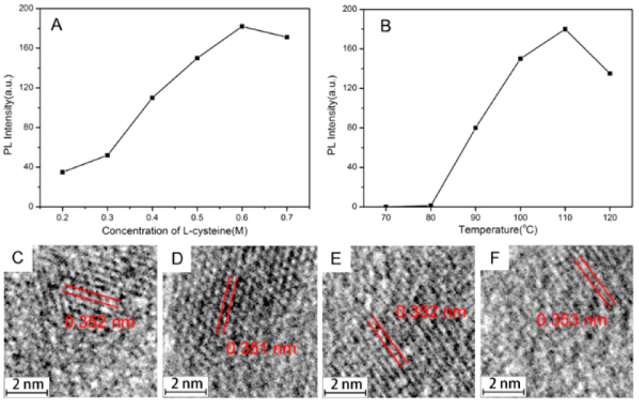

Figure 3. Dependence of PL intensity upon concentration of L-cysteine (A) and reaction temperature (B) for the case of [Ag]/[Zn] = 1/6; HRTEM images of samples synthesized at 90 °C (C), 100 °C (D), 110 °C (E), 120 °C (F).

continuous increase of the concentration of L-cysteine, which confirms that the surface of ZAIS QDs is stabilized by L-cysteine ligand since the dangling bonds and vacancies are passivated. Intriguingly, an excess amount of ligand can result in reduction of PL intensity as the concentration is 0.7 M. We speculate that this may contribute to the formation of new nonradiative recombination sites because of the excess ligand on the surface.

3.2.2. Effect of Reaction Temperature. The PL intensity of the resulting ZAIS QDs was found to be strongly dependent on the reaction temperature (Figure 3B). With an increase of the reaction temperature (70−110 °C), the PL intensity is enhanced systematically. If the reaction temperature is too low (below 80 °C), no evident PL emission is found, since it does not form ZAIS QDs. As for a higher temperature, such as 120 °C, the PL intensity was decreased obviously. Since the XRD patterns of the samples are broad (see Morphology and Structure Characterization), we measured the HRTEM to study the crystallinity of each sample synthesized under different temperature conditions (90, 100, 110, 120 °C). As shown in Figure 3C−E, the HRTEM images show clear lattice fringes, while in Figure 3F, the fringes are ambiguous, indicating the poor crystallinity of the samples prepared at 120 °C. This may be because the growth rate of nanocrystals was too fast at higher temperature (120 °C), forming a lot of structure defects and giving rise to fluorescence quenching. Therefore, we make use of a Teflon-lined autoclave to create a reaction environment of 110 °C to improve PL intensity. Because of the high temperature as well as the high pressure generated by the sealed autoclave, the QDs have a nice crystallinity. Thus, a high QY of 26% is achieved.

3.3. ZAIS/ZnS Core/Shell Structure. The ZAIS/ZnS core/shell structure NCs were formed in situ on the as prepared ZAIS QDs. It is known that robust shells can impart to QDs chemical and physical stability and gain higher quantum yield of emission. Modifying with ZnS, which is an excellent candidate for its wide band gap (bulk E_g = 3.68 eV), is frequently used to passivate the surface and enhance the stability of many kinds of nanoparticles, such as CdS and CdSe.[36] Figure 4A shows the temporal evolution of PL

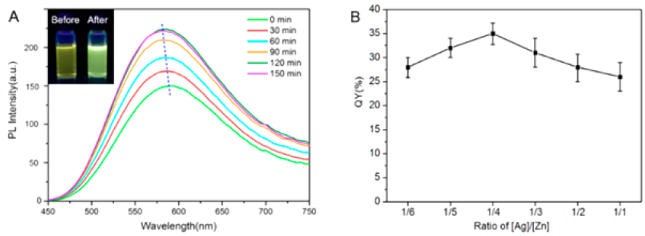

Figure 4. (A) Evolution of PL emission with reaction time of ZnS coating (inset: digital picture of ZAIS before and after coating with ZnS taken under the UV light); (B) QY of ZAIS/ZnS NCs of each sample.

emission. The inset of a digital camera picture acquired before and after the capping process gives us visualized images of increasing emission. As we can see from the curves, there is an enhancement of PL intensity of 1.5-fold from 0 to 120 min, illustrating that surface defects of ZAIS including dangling bonds and vacancies are eliminated by means of the passivation of ZnS shell. The slight blue shift is probably caused by the diffusion of Zn into ZAIS QDs, broadening the band gap of the NCs. The decrease of emission maximum at 150 min is similar to ZAIS, which may partly contribute to the formation of new defect states arising from the mismatch of the core/shell structure with the further thickening of the ZnS shell, resulting in nonradiation recombination of carriers. Another reason may be the further reduction of the intrinsic point defects, which act as deep donor−acceptor pairs, via cation exchange of Ag ions by Zn.[24] Figure 4B shows the QY of ZAIS/ZnS of each case. All

DOI: 10.1021/ic502600u
Inorg. Chem. 2015, 54, 1627−1633

the samples were found to have improvement of PL intensity and QY after coating with ZnS, elucidating that a proper thickness of the ZnS shell can indeed ameliorate the optical properties.

3.4. PL Relaxation of ZAIS QDs and ZAIS/ZnS NCs. To further gain the mechanism of electron−hole recombination, we measured time-resolved PL spectra of samples ([Ag]/[Zn] = 1/6), as is presented in Figure 5. The PL decay curve of each

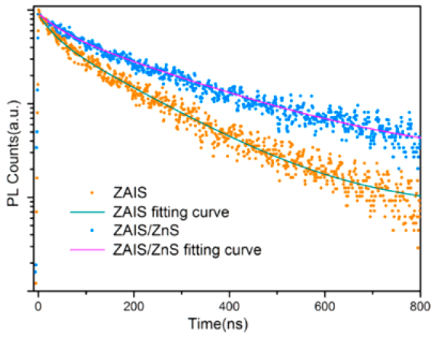

Figure 5. PL lifetime spectra of ZAIS and ZAIS/ZnS with [Ag]/[Zn] = 1/6.

sample can be well fitted by a biexponential function $I(t) = y_0 + B_1 \exp(-t/\tau_1) + B_2 \exp(-t/\tau_2)$, where $I(t)$ is the PL intensity at delay time (t), B_1 and B_2 represent the relative weights of the decay components at $t = 0$, and τ_1 and τ_2 are the lifetimes. These constants coupled with effective decay lifetimes, which could be calculated using the equation $t = (B_1\tau_1^2 + B_2\tau_2^2)/(B_1\tau_1 + B_2\tau_2)$,[37] are listed in Table 2. As we know, different electron−

Table 2. PL Decay Constants Obtained from $I(t) = y_0 + B_1 \exp(-t/\tau_1) + B_2 \exp(-t/\tau_2)$

samples	lifetime/ns	τ_1/ns	B_1	τ_2/ns	B_2
ZAIS	130.5	28.6	0.36	144.1	0.54
ZAIS/ZnS	206.9	41.5	0.31	222.7	0.60

hole recombination mechanisms bring about the distinct PL decay time. It is reported that the fast decay component can be attributed to intrinsic recombination, while the slow component can be ascribed to defect-related recombination of carriers.[38] In our case, the shorter and the longer lifetime can be assigned to surface trap states and donor−acceptor transition of trap (intrinsic) states, respectively.[6,27] Table 2 shows that the weight of the slow decay component is considerably larger than that of the fast decay component, which illustrates that PL emission is mainly composed of the intrinsic states. This conclusion is also in good agreement with the results of deconvolution which is discussed in Optical Properties, and could explain the broad fwhm of emission. After the ZAIS core is coated with the ZnS shell, the fast decay component is increased and its contribution to the whole emission is decreased, which indicates that the surface defect is effectively suppressed by ZnS, getting longer average lifetime of 206.9 ns than that of ZAIS QDs (130.5 ns).

3.5. Morphology and Structure Characterization. The crystal structures of the samples were investigated by XRD with Cu Kα radiation. Figure 6A shows the XRD patterns for the ZAIS QDs of the samples with [Ag]/[Zn] = 1:0, 1:1, 1:3, and 1:5. The peaks of [Ag]/[Zn] = 1:0, i.e., Ag−In−S nanocrystals, basically match the characteristic peaks of cubic $AgIn_5S_8$. Due

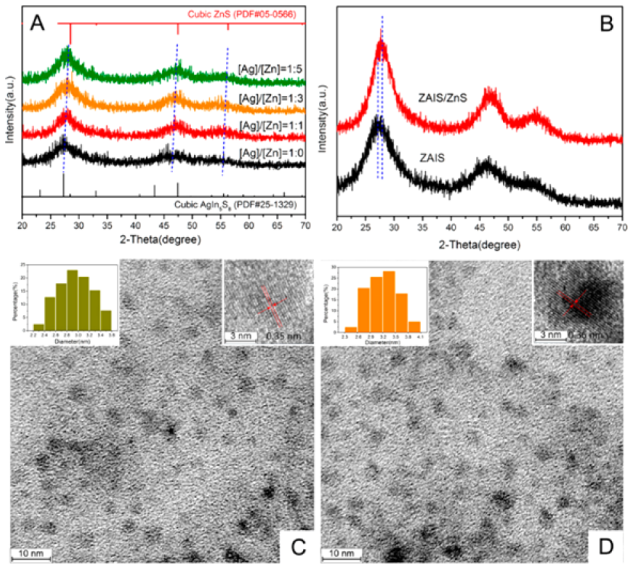

Figure 6. XRD patterns of ZAIS nanocrystals with [Ag]/[Zn] = 1:0, 1:1, 1:3, and 1:5, respectively (A); XRD patterns of ZAIS core and ZAIS/ZnS NCs with [Ag]/[Zn] = 1/3 (B); TEM images of ZAIS core with [Ag]/[Zn] = 1/3 (C) and corresponding ZAIS/ZnS core/shell NCs (D). Insets: Corresponding histograms of size distribution (top left) and HRTEM (top right) images of the sample.

to their small particle size, all of the curves exhibit three broad and weak peaks. All the peaks of the samples are located between the corresponding peaks of bulk cubic $AgIn_5S_8$ and ZnS, and shifted to higher angle with the decrease of the ratio of [Ag]/[Zn] because of the increasing component of ZnS.[15,39] After coating with ZnS shell, because the lattice constant is bigger than that of ZAIS, the diffraction peaks similarly shifted to larger angles (Figure 6B), indicating that these samples are not a simple mixture of ZnS and $AgIn_5S_8$ but a formation of quaternary ZAIS QDs and ZAIS/ZnS core/shell structure.

TEM observation (Figures 6C and 6D) reveals that both of the NCs have remarkable monodispersity. The average size of the sphere-shaped NCs is determined to be 3.0 and 3.2 nm, respectively, based on the static analysis of more than 100 particles in a certain region. The histograms of size distribution are given in the insets of Figures 6C and 6D, exhibiting relatively wide distribution. The HRTEM images lying in the top-right insets of Figures 6C and 6D show continuous lattice fringes, which are indicatives of the single crystalline nature of the NCs. Because of the finite size, the small thickness, and the resolution limit of the instrument, we cannot distinguish the ZnS shell from the ZAIS core. EDS and XPS FTIR analysis, which were further worked to determine the elements and their molar ratio and to certify the stabilizer on the surface of the nanocrystals, is presented in the Supporting Information.

3.6. *In Vitro* Cytotoxicity. It is of great importance to evaluate the *in vitro* cytotoxicity of our prepared ZAIS QDs and ZAIS/ZnS NCs before applying them as fluorescent probes in bioimaging. A standard cell viability assay based on 1-methyltetrazole-5-thiol (MTT) was performed on Hep G2 cells that are meant to be used for imaging. The concentration-dependent effect of ZAIS/ZnS QDs at 24 h was determined. As is depicted in Figure 7, the cell viability of L-cysteine terminated CdTe/ZnS QDs synthesized by Mntungwa's method is 80% at a concentration of 0.3 mg/mL, and decreased rapidly with the further increase of the concentration. Differently, the L-cysteine

DOI: 10.1021/ic502600u
Inorg. Chem. 2015, 54, 1627−1633

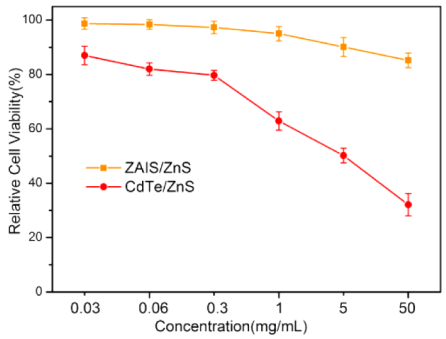

Figure 7. *In vitro* cytotoxicity of the aqueous L-cysteine-capped ZAIS/ZnS QDs and L-cysteine-capped CdTe/ZnS QDs determined by MTT assay.

terminated ZAIS/ZnS NCs show a cell viability up to 85% even at a high concentration of 50 mg/mL after being incubated for 24 h. What is more, ZnS shell prevents the Ag^{+} or In^{3+} exudating from the ZAIS core and further reduces the cytotoxicity. Such a low cytotoxicity *in vitro* reveals that L-cysteine stabilized ZAIS/ZnS provide a necessary precondition for the high biocompatibility *in vivo* and can be used as intracellular markers for clinical diagnosis.

3.7. Specific Cellular Labeling and Imaging with ZAIS/ZnS NCs. Nowadays, hepatocellular carcinoma (HCC) is becoming a global health concern which is mainly the consequence of hepatitis B and hepatitis C. In clinical diagnosis, alpha-fetoprotein (AFP) concentration is a significant indicator for the reason that AFP is a highly specific marker for HCC.[40] In consideration of PL intensity and cytotoxicity, yellow emission ZAIS/ZnS core/shell QDs-linked AFP antibodies were applied to specifically mark the AFPs which extensively exist in HCC cells. A schematic diagram of the linkage between AFP antibodies and ZAIS/ZnS QDs and delivery to cells is presented in Scheme 2. In general, antibody is a globulin which is composed of four polypeptide chains covalently bound via disulfide bridges. The whole antibody is divided into two parts,

Scheme 2. Schematic Diagram of the Linkage between AFP Antibodies and ZAIS/ZnS QDs and Delivery to Cells

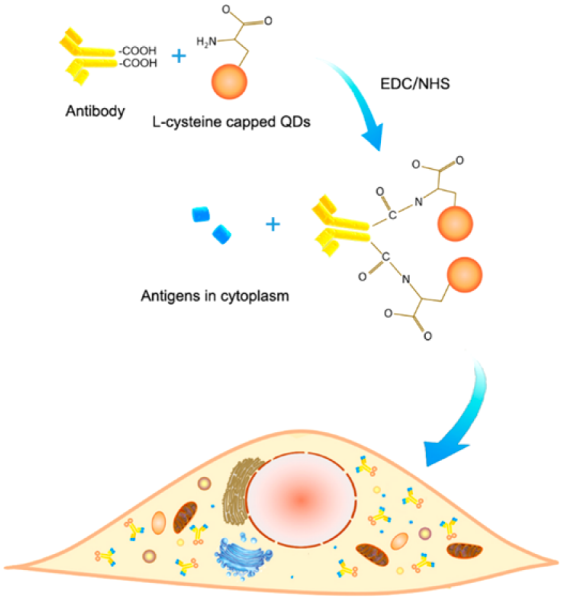

i.e., variable region and constant region. The ends of the constant region are terminated by carboxyl groups which could react to amino groups of L-cysteine located in the surface of QDs to produce amide bond according to EDC/NHS protocol.[41,42] The QDs/antibody composites are delivered into Hep G2 cells and specifically bound to AFP antigen. Figures 8A and 8B show the images under ambient light and

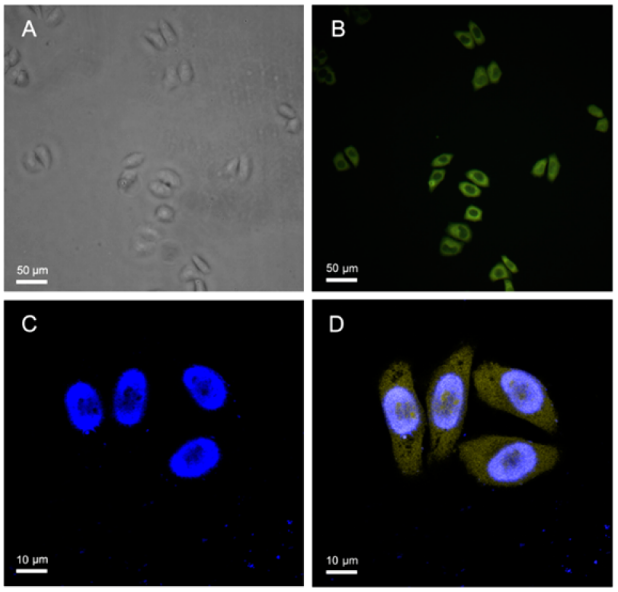

Figure 8. Bright-field (A) and fluorescent image of Hep G2 cells under excitation at 360 nm (B); confocal laser-scanning fluorescent microscopy images of Hep G2 cells stained by DAPI with 430−470 nm (C) and 430−590 nm (D) bandpass filters.

UV light of Hep G2 cells, respectively. The normal cellular morphology under visible light reveals marvelous biocompatibility of L-cysteine stabilized ZAIS/ZnS NCs. For the purpose of observing the DAPI stained and QD/antibody composite labeled Hep G2 cells more clearly and delicately, laser scanning confocal microscopy is performed for image collection. Figure 8C is the picture taken on the condition of blue channel in which we can see the blue emission only, showing a legible profile of the nucleus. Figure 8D gives the image photographed on the blue and yellow channels simultaneously, showing the QD-marked cytoplasm and DAPI stained nucleus distinctly. All of the fluorescent and confocal images indicate that AFP antibodies have been specifically bound to the antigen receptor in the cytoplasm of Hep G2 cells. To the best of our knowledge, this is the first report on labeling of HCC cytoplasm using fluorescent quaternary QDs, and clarified capacity of the core/shell-structured ZAIS/ZnS nanoparticles in targeted cellular imaging and monitoring.

4. CONCLUSIONS

In summary, Zn-doped $AgIn_5S_8$ nanocrystals have been conveniently prepared via a one-step approach of reaction between metal salt and TAA with L-cysteine as ligands on the surface. The emission wavelength can be tuned conveniently by the variation of the stoichiometric ratio of [Ag]/[Zn]. The concentration of L-cysteine and the temperature have significant influence on the PL intensity. As the reaction progresses, the number of shallow surface defects in high energy was lowered relatively, and intrinsic state recombination dominates the PL

DOI: 10.1021/ic502600u
Inorg. Chem. 2015, 54, 1627−1633

emission. After coating with a ZnS shell, the PL QY increased substantially to 26−35% and obtained longer PL lifetime. Besides the prominent optical properties, the obtained ZAIS/ZnS NCs also exhibit excellent biocompatibility in the studies of cytotoxicity. Furthermore, the as prepared NCs were conjugated to AFP antibody and realized targeted labeling and imaging, indicating the promising application of monitoring single-cell level.

■ ASSOCIATED CONTENT

Supporting Information

EDS, XPS, and FTIR analysis of as prepared ZAIS/ZnS core/shell nanocrystals. This material is available free of charge via the Internet at http://pubs.acs.org.

■ AUTHOR INFORMATION

Corresponding Authors

*E-mail: xlxu@ustc.edu.cn (X.X.).
*E-mail: xrx2041@163.com (R.X.).
*E-mail: lx-zhu@163.com (L.Z.).

Notes

The authors declare no competing financial interest.

■ ACKNOWLEDGMENTS

Financial support by the National Natural Science Foundation of China (No. 51272246) and Scientific and Technological Research Foundation of Anhui (No. 12010202035) is appreciatively acknowledged.

■ REFERENCES

(1) Chang, J.-Y.; Wang, G.-Q.; Cheng, C.-Y.; Lin, W.-X.; Hsu, J.-C. *J. Mater. Chem.* **2012**, *22* (21), 10609.
(2) Dai, M.-l.; Okazaki, K.-i.; Kudo, A.; Kuwabata, S.; Torimoto, T. *Electrochemistry* **2011**, *10*, 790.
(3) Li, T.-L.; Teng, H. *J. Mater. Chem.* **2010**, *20* (18), 3656.
(4) Luo, Z.; Zhang, H.; Huang, J.; Zhong, X. *J. Colloid Interface Sci.* **2012**, *377* (1), 27.
(5) Takahashi, T.; Kudo, A.; Kuwabata, S.; Ishikawa, A.; Ishihara, H.; Tsuboi, Y.; Torimoto, T. *J. Phys. Chem. C* **2012**, *117* (6), 2511.
(6) Tang, X.; Ho, W. B. A.; Xue, J. M. *J. Phys. Chem. C* **2012**, *116* (17), 9769.
(7) Tsuji, I.; Kato, H.; Kudo, A. *Angew. Chem.* **2005**, *117* (23), 3631.
(8) Tsuji, I.; Kato, H.; Kudo, A. *Angew. Chem., Int. Ed.* **2005**, *44* (23), 3565.
(9) Tsuji, I.; Kato, H.; Kudo, A. *Chem. Mater.* **2006**, *18* (7), 1969.
(10) Zhang, W.; Zhong, X. *Inorg. Chem.* **2011**, *50* (9), 4065.
(11) Hong, K. J.; Jeong, J. W.; Jeong, T. S.; Youn, C. J.; Lee, W. S.; Park, J. S.; Shin, D. C. *J. Phys. Chem. Solids* **2003**, *64* (7), 1119.
(12) Hong, S. P.; Park, H. K.; Oh, J. H.; Yang, H.; Do, Y. R. *J. Mater. Chem.* **2012**, *22* (36), 18939.
(13) Mao, B.; Chuang, C.-H.; Wang, J.; Burda, C. *J. Phys. Chem. C* **2011**, *115* (18), 8945.
(14) Zhong, H.; Bai, Z.; Zou, B. *J. Phys. Chem. Lett.* **2012**, *3* (21), 3167.
(15) Tang, X.; Yu, K.; Xu, Q.; Choo, E. S. G.; Goh, G. K. L.; Xue, J. *J. Mater. Chem.* **2011**, *21* (30), 11239.
(16) Regulacio, M. D.; Win, K. Y.; Lo, S. L.; Zhang, S.-Y.; Zhang, X.; Wang, S.; Han, M.-Y.; Zheng, Y. *Nanoscale* **2013**, *5* (6), 2322.
(17) Qu, L.; Peng, X. *J. Am. Chem. Soc.* **2002**, *124* (9), 2049.
(18) Mntungwa, N.; Rajasekhar Pullabhotla, V. S.; Revaprasadu, N. *Colloids Surf., B* **2013**, *101* (0), 450.
(19) Jiang, T.; Yin, N.; Liu, L.; Song, J.; Huang, Q.; Zhu, L.; Xu, X. *RSC Adv.* **2014**, *4* (45), 23630.
(20) Parsons, J. G.; Dokken, K. M.; McClure, J.; Gardea-Torresdey, J. L. *Polyhedron* **2013**, *56* (0), 237.
(21) Soomro, R. A.; Nafady, A.; Sirajuddin; Memon, N.; Sherazi, T. H.; Kalwar, N. H. *Talanta* **2014**, *130* (0), 415.
(22) Stevenson, A. W.; Milanko, M.; Barnea, Z. *Acta Crystallogr., B* **1984**, *B40*, 521.
(23) Hamanaka, Y.; Ogawa, T.; Tsuzuki, M.; Kuzuya, T. *J. Phys. Chem. C* **2011**, *115* (5), 1786.
(24) Mao, B.; Chuang, C.-H.; Lu, F.; Sang, L.; Zhu, J.; Burda, C. *J. Phys. Chem. C* **2013**, *117* (1), 648.
(25) Tsuji, I.; Kato, H.; Kobayashi, H.; Kudo, A. *J. Am. Chem. Soc.* **2004**, *126* (41), 13406.
(26) Dai, M.; Ogawa, S.; Kameyama, T.; Okazaki, K.-i.; Kudo, A.; Kuwabata, S.; Tsuboi, Y.; Torimoto, T. *J. Mater. Chem.* **2012**, *22* (25), 12851.
(27) Torimoto, T.; Ogawa, S.; Adachi, T.; Kameyama, T.; Okazaki, K.-i.; Shibayama, T.; Kudo, A.; Kuwabata, S. *Chem. Commun.* **2010**, *46* (12), 2082.
(28) Burda, C.; Chen, X.; Narayanan, R.; El-Sayed, M. A. *Chem. Rev.* **2005**, *105* (4), 1025.
(29) Karar, N.; Singh, F.; Mehta, B. R. *J. Appl. Phys.* **2004**, *95* (2), 656.
(30) McKinnon, A. E.; Szabo, A. G.; Miller, D. R. *J. Phys. Chem.* **1977**, *81* (16), 1564.
(31) Guyot-Sionnest, P.; Hines, M. A. *Appl. Phys. Lett.* **1998**, *72* (6), 686.
(32) Guyot-Sionnest, P.; Shim, M.; Matranga, C.; Hines, M. *Phys. Rev. B* **1999**, *60* (4), R2181.
(33) Deng, D.; Cao, J.; Qu, L.; Achilefu, S.; Gu, Y. *Phys. Chem. Chem. Phys.* **2013**, *15* (14), 5078.
(34) Eychmüller, A. *J. Phys. Chem. B* **2000**, *104* (28), 6514.
(35) Wang, D.; Zheng, W.; Hao, C.; Peng, Q.; Li, Y. *Chem. Commun.* **2008**, *22*, 2556.
(36) Samanta, A.; Deng, Z.; Liu, Y. *Langmuir* **2012**, *28* (21), 8205.
(37) Wu, L.; Ji, M.; Wang, H.; Kong, Y.; Zhang, Y. *Opt. Mater. Express* **2014**, *4* (8), 1535.
(38) Xiang, W.; Xie, C.; Wang, J.; Zhong, J.; Liang, X.; Yang, H.; Luo, L.; Chen, Z. *J. Alloys Compd.* **2014**, *588* (0), 114.
(39) Torimoto, T.; Adachi, T.; Okazaki, K.-i.; Sakuraoka, M.; Shibayama, T.; Ohtani, B.; Kudo, A.; Kuwabata, S. *J. Am. Chem. Soc.* **2007**, *129* (41), 12388.
(40) Li, D.; Mallory, T.; Satomura, S. *Clin. Chim. Acta* **2001**, *313* (1−2), 15.
(41) Di Corato, R.; Bigall, N. C.; Ragusa, A.; Dorfs, D.; Genovese, A.; Marotta, R.; Manna, L.; Pellegrino, T. *ACS Nano* **2011**, *5* (2), 1109.
(42) Xie, M.; Hu, J.; Long, Y.-M.; Zhang, Z.-L.; Xie, H.-Y.; Pang, D.-W. *Biosens. Bioelectron.* **2009**, *24* (5), 1311.

DOI: 10.1021/ic502600u
Inorg. Chem. 2015, 54, 1627−1633